Location Parameter Estimation of Moving Aerial Target in Space-Air-Ground Integrated Networks-Based IoV

Mingqian Liu, *Member, IEEE,* Bo Li, *Member, IEEE,* Yunfei Chen, *Senior Member, IEEE,* Zhutian Yang, *Senior Member, IEEE,* Nan Zhao, *Senior Member, IEEE,* Peng Liu, and Fengkui Gong, *Member, IEEE*

***Abstract*—Estimating the location parameters of moving target is an important part of intelligent surveillance for Internet of Vehicles (IoV). Satellite has the potential to play a key role in many applications of space-air-ground integrated networks (SAGIN). In this paper, a novel passive location parameter estimator using multiple satellites for moving aerial target is proposed. In this estimator, the direct wave signals in reference channels are first filtered by a band-pass filter, followed by a sequence cancellation algorithm to suppress the direct-path interference and multi-path interference. Then, the fourth-order cyclic cumulant cross ambiguity function (FOCCCAF) of the signals in the reference channels and the four-weighted fractional Fourier transform fourth-order cyclic cumulant cross-ambiguity function (FWFRFT-FOCCCAF) of signals in the surveillance channels are derived. Using them, the time difference of arrival (TDOA) and the frequency difference of arrival (FDOA) are estimated and the distance between the target and the receiver and the velocity of the moving aerial target are estimated by using multiple satellites. Finally, the Cramer-Rao Lower Bounds of the proposed location parameter estimators are derived to benchmark the estimator. Simulation results show that the proposed method can effectively and precisely estimate the location parameters of the moving aerial target.**

***Index Terms*—Frequency difference of arrival, Internet of vehicles, location parameter estimation, space-air-ground integrated networks, time difference of arrival.**

I. Introduction

THE development of internet of Vehicles (IoV) and mobile edge computing networks leads to urgent demand for broadband access capability [1]-[2]. At the same time, the use of satellites is found to be of paramount importance in IoV, such as intelligent surveillance. Thus, satellite-based IoV is viewed as a vital part of space-air-ground integrated networks (SAGIN) to provide broadband access [3]-[5]. Data transmission and radar sensing are useful tools to extract valuable information from the environment [6]-[7]. Among them, passive location systems utilize the reflected echo signals from a moving target generated by a non-cooperative radiation source for parameter estimation. As a result, moving target passive location using an external radiation source has been extensively studied [8]-[9].

To realize effective moving target passive localization, the time difference of arrival (TDOA) and the frequency difference of arrival (FDOA) are often accurately estimated first to acquire useful information, including the distance and velocity of the moving target for further tracking and positioning. In recent years, much research effort has spent on TDOA and FDOA estimation using satellite illuminator. The authors in [10] proposed a TDOA estimator of GNSS signal using the tensor-based filtering approach, in which the highly correlated signal and noise components are separated using singular value decomposition and spatial smoothing. After filtering weak echo signals, cross correlation with the direct wave signal was used to obtain the TDOA. This method had a high computational complexity due to the matrix processing. In [11], FDOA estimation combining zero forcing and double fast Fourier transform was proposed to tackle the poor accuracy of the FDOA estimation for GNSS signals. However, the estimation performance still poor for low input signal to interference plus noise ratio. In [12], an FDOA estimation method with optical phase-locked loop and broadcast ephemeris of GPS was proposed. This method had poor adaptability and universality since it was sensitive to the change of satellite orbit and elevation angle. An FDOA estimation method for GNSS echo signal based on fast Fourier transform (FFT) was proposed in [13], and this method can reduce the computational complexity. However, it did not consider the influence of noise on the estimation. As for the TDOA and FDOA estimation using multiple satellites, the authors in [14] proposed a method of passive location with multi-GNSS, but the method only works for geometric modeling. Notably, the works mentioned above only studied the TDOA or FDOA estimation methods using the radiation source of a single satellite, which often has small coverage, low reliability, as well as limited applications and geographical environments. In practice, a receiver may

This work was supported by the National Natural Science Foundation of China under Grant 62071364, in part by the Aeronautical Science Foundation of China under Grant 2020Z073081001, in part by the Fundamental Research Funds for the Central Universities under Grant JB210104, in part by the Shaanxi Provincial Key Research and Development Program under Grant 2019GY-043, and in part by the 111 Project under Grant B08038. *(Corresponding author: Bo Li.)*

M. Liu, P. Liu and F. Gong are with the State Key Laboratory of Integrated Service Networks, Xidian University, Shaanxi, Xi'an 710071, China (e-mail: mqliu@mail.xidian.edu.cn; nx_liupeng@126.com; fkgong@xidian.edu.cn).

B. Li is with the School of Information Science and Engineering, Harbin Institute of Technology at Weihai, Weihai 264209, China (email: libo1983@hit.edu.cn).

Y. Chen is with the School of Engineering, University of Warwick, Coventry, West Midlands United Kingdom of Great Britain and Northern Ireland CV4 7AL (e-mail: yunfei.chen@warwick.ac.uk).

Z. Yang is with the School of Electronics and Information Engineering, Harbin Institute of Technology, Harbin 150001, China (e-mail: yangzhutian@hit.edu.cn).

N. Zhao is with the School of Information and Communication Engineering, Dalian University of Technology, Dalian 116024, China. (email: zhaonan@dlut.edu.cn).

receive radiation signals from multiple satellites of different types at the same time. As a result, previous works using a single satellite on target detection and parameter estimation may not work well due to the detrimental interference from other satellites. Therefore, in this paper, we study the location parameter estimation in the presence of multiple satellites to improve the estimation accuracy.

Specifically, considering multiple satellites, location parameter estimation methods based on fourth-order cyclic cumulant cross ambiguity function (FOCCCAF) and four-weighted fractional Fourier transform fourth-order cyclic cumulant cross ambiguity function (FWFRFT-FOCCCAF) are proposed in this paper. The main contributions of this paper are summarized as follows:

- The statistics for parameter estimation with multiple weak echo signals are obtained using the signal cyclostationarity. The weighted fractional Fourier transform (WFRFT) will be used to reduce the degree of coupling between the signal and interference for interference suppression.
- TDOA and FDOA estimation method are proposed to extract the spectral peak-values from the the statistics for parameter estimation.
- The proposed method requires multi-satellite collaboration through data fusion to estimate the distance from a moving aerial target to a receiver as well as its velocity.

The reminder of the paper is organized as follows. Section II shows the system model. In Section III, the joint passive location parameter estimation method is proposed. Section IV presents the Cramer-Rao lower bounds for location parameter estimators. In Section V, simulation results are provided. Finally, Section VI concludes the paper.

II. System Model

The moving aerial target localization system for SAGIN-based IoV is shown in Fig. 1. Signal form the satellite illuminators signals are received in both surveillance channel and reference channel. The reference channel is composed of omnidirectional antennas at the vehicle, which receives the satellite illuminator signal for positioning as baseline measurements. On the other hand, the surveillance channel is composed of directional antennas at the vehicle, which receives the weak echo signal of a moving aerial target in the presence of direct-path interference (DPI) and multi-path interference (MPI). The signal processing module is used to process the received signals and analyze the correlation between the reference channel and surveillance channel. The surveillance channel reflected echo signal contains a receiving antenna, an amplifier, a filter, a down conversion circuit, and a digital storage oscilloscope. In addition to the reflected echoes received by the plurality of satellite signals from the target, DPI and MPI occur in the surveillance channel.

The signal in the reference channel is given by [15]

$$x(t) = \sum_{i=1}^{M'} r_i s_i(t) + n\,(t)\,, \tag{1}$$

where M' is the number of satellites, $s_i(t)$ and r_i represent the ith satellite illuminator direct wave signal and its amplitude, respectively, and $n\,(t)$ stands for the complex zero-mean white Gaussian noise in the reference channel.

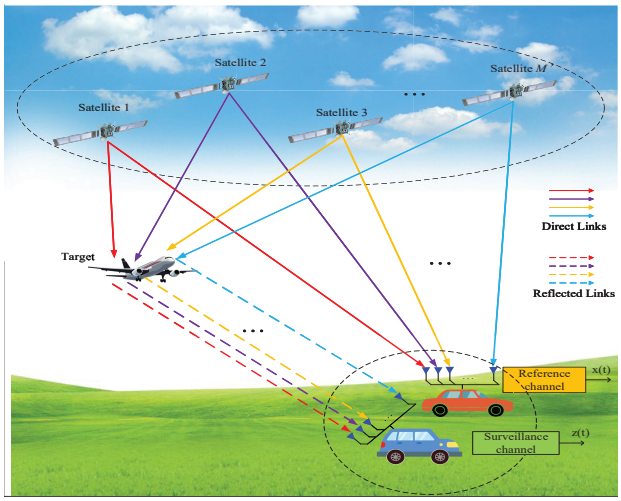

Fig. 1. Location system model in space-air-ground integrated networks-based IoV.

The signal in the surveillance channel is

$$\begin{aligned} z(t) = &\sum_{\eta=1}^{M'} r'_\eta s_\eta(t - D_\eta) e^{-j2\pi f_{d_\eta} t} + \sum_{\eta=1}^{M'} \Omega_\eta s_\eta(t) \\ &+ \sum_{\eta=1}^{M'} \sum_{j=1}^{H} \omega_{\eta j} s_\eta(t - \tau_{\eta j}) + n'(t) \quad , \end{aligned} \tag{2}$$

where r'_η is the amplitude of the ηth weak echo signal, D_η and f_{d_η} stand for its TDOA and FDOA, respectively, Ω_η is the amplitude of ηth direct wave signal in the surveillance channel, H represents the number of multipath components in the surveillance channel, $\omega_{\eta j}$ and $\tau_{\eta j}$ are the amplitude and time delay of the ηth direct wave signal through the jth multipath, respectively. In addition, $n'(t)$ is the complex zero-mean white Gaussian noise in the surveillance channel.

III. Joint Location Parameter Estimation for Moving Aerial Target

In this section, the sequence cancellation algorithm will be employed to suppress DPI and MPI. Afterwards, DOA and FDOA will be estimated by FOCCCAF and FWFRFT-FOCCCAF, and data fusion method will be utilized to estimate the velocity and distance of the moving target.

A. DPI and MPI Suppression in the Surveillance Channel

The receiver in the reference channel receives multiple different direct wave signals at the same time. Thus, it is necessary to separate them first to provide reference signals, in order to suppress DPI and MPI in the surveillance channel. As the frequencies of different satellite signals are different, a band-pass filter can be used to separate the multiple direct wave signals in the reference channel. The transfer function of the band-pass filter $H(e^{j\omega})$ is [16]:

$$H(e^{j\omega}) = \frac{\sum_{r=0}^{E} b_r \left(e^{j\omega}\right)^{-r}}{1 + \sum_{k=1}^{S} a_k (e^{j\omega})^{-k}}, \tag{3}$$

where a_k and b_r are the coefficients for the band-pass filter. The separation of different direct wave signals in the reference channel can be achieved by using several parallel filters, whose parameters should be chosen according to the operating frequency spectrum ranges, and the values of E, S, a_k and b_r of the bandpass filters should be carefully selected. After band-pass filtering, the reference channel signals are converted into M direct wave signals uncoupled with each other. The ith satellite radiation direct wave signal after separation can be expressed as

$$x_i(t) = r_i s_i(t) + n_i(t). \tag{4}$$

We propose a multi-sequence cancellation algorithm (M-SCA), which is able to simultaneously suppress the interference caused by multiple direct wave signals and multi-path signals in the surveillance channel [17], [18]. First of all, the direct wave signals in the reference channel and the weak echo in the surveillance channel are sampled, giving

$$x_i = [x_i[-R+1], x_i[-R+2], \ldots, x_i[N-1]]^T, \tag{5}$$

where $i = 1, 2, 3, \ldots, M$ and M is the number of direct wave signals, x_i denotes the ith direct wave signal, N is the number of sampling points, R stands for the sampling point where the reference signal is more than the surveillance channel signal, $x_i[\cdot]$ represents the different sampling points of the i_{th} direct wave. Similarly, the signal vector in the surveillance channel after sampling can be expresses as

$$z = [z[0], z[1], \ldots, z[N-1]]^T. \tag{6}$$

To reduce the problem with large the computational complexity, the original direct wave signals and surveillance channel signals are segmented. Let $N_B = N/b$ be the length of each segment, where N and b are the total length of the original signal and the number of segments, respectively. The segmented signals are

$$x_i' = \left[x_{i_0}^T, x_{i_1}^T, \ldots, x_{i_{b-1}}^T\right]^T, \tag{7}$$

$$z' = \left[z_0^T, z_1^T, \ldots, z_{b-1}^T\right]^T, \tag{8}$$

where

$$x_{i_k} = [x_i[kN_B - R + 1], \ldots, x_{i_k}[(k+1)N_B - 1]]^T, \tag{9}$$

$$z_k = [z_k[kN_B], \ldots, z_k[(k+1)N_B - 1]]^T, \tag{10}$$

and $k = 0, 1, \ldots, b-1$. The signal in the surveillance channel after DPI and MPI suppression can be expressed as

$$z_{MSCA-B} = \left[z_{SCA-B_0}^T, z_{SCA-B_1}^T, \ldots, z_{SCA-B_{b-1}}^T\right]^T, \tag{11}$$

where $z_{SCA-B_i} (i = 0, 1, \ldots, b-1)$ is

$$z_{SCA-B_i} = Q_1 Q_2 \ldots Q_M z', \tag{12}$$

$$Q_j = I_N - \frac{\tilde{x}_{j-1} \cdot \tilde{x}_{j-1}^H}{\tilde{x}_{j-1}^H \cdot \tilde{x}_{j-1}}, \tag{13}$$

$$\tilde{x}_{j-1} = P_j x_{j-1}, \tag{14}$$

$$P_M = I_N, \tag{15}$$

$$P_j = Q_{j+1} Q_{j+2} \ldots Q_M, \tag{16}$$

and x_{j-1} is the jth column of matrix X_k. Also,

$$X_k = [Bx''_{1_k}, Bx''_{2_k}, Bx''_{3_k}, \ldots, Bx''_{M_k}], \tag{17}$$

$$B = \{\ b_{mn}\ \}, b_{mn} = \begin{cases} 1\ , & m = n - R + 1, \\ 0\ , & else, \end{cases} \tag{18}$$

and $m = 1, 2, \ldots, N_B$,

$$x''_{i_k} = \left[x_{i_k}, Dx_{i_k}, D^2 x_{i_k}, \ldots, D^{T_{\max}-1} x_{i_k}\right], \tag{19}$$

$i = 1, 2, \ldots, M$, $k = 0, 1, \ldots, b-1$,

$$D = \{\ d_{mn}\}_{m,n=1,2,\ldots,N_B+R-1}, d_{ij} = \begin{cases} 1\ , & m = n+1, \\ 0\ , & else, \end{cases} \tag{20}$$

where $T_{\max} = L_{\max}/c$ is the maximum of TDOA, $L_{\max}$ is the maximum detection distance, and c is the speed of light in free space.

We use $y(t)$ to represent the signal in the surveillance channel after the suppression of DPI and MPI as

$$y(t) = \sum\nolimits_{\eta=1}^{M'} r'_\eta s_\eta (t - D_\eta) e^{-j2\pi f_{d_\eta} t} + n'(t). \tag{21}$$

B. TDOA and FDOA Estimation

1) Fourth-Order Cyclic Cumulant Cross Ambiguity Function: The signals possess the characteristics of cyclic stationary and the cross ambiguity function can reflect the time-frequency characteristics of the signal. The cross ambiguity function using the fourth-order cyclic cumulant of the direct wave signal and the weak echo signal are [19]

$$\chi_{y,x_i}^{\alpha_i - f, \alpha_i}(u, f) = \int_{-\infty}^{+\infty} C_{x_i x_i x_i y}^{\alpha_i - f}(\tau) C_{4x_i}^{\alpha_i}(\tau - u)^* e^{j\pi f \tau} d\tau, \tag{22}$$

where $C_{4x_i}^{\alpha_i}(\tau)$ is the fourth-order self-cyclic cumulant of $x_i(t)$ when the cycle frequency is α_i, and $C_{x_i x_i x_i y}^{\alpha_i - f}(\tau)$ is the fourth-order cross-cyclic cumulant of $x_i(t)$ and $y(t)$ when the cycle frequency is $\alpha_i - f$, $C_{4x_i}^{\alpha_i}(\tau)$ is given by

$$C_{4x_i}^{\alpha_i}(\tau) = r_i^4 M_{4s_i}^{\alpha_i}(\tau) - 3A r_i^2 M_{2s_i}^{\alpha_i}(\tau), \tag{23}$$

where $A = E[s_i^2(t)]$, $M_{4s_i}^{\alpha_i}(\tau)$ and $M_{2s_i}^{\alpha_i}(\tau)$ are the fourth-order self-cyclic moment and second-order self-cyclic moment of $s_i(t)$, which can be obtained as

$$M_{4s_i}^{\alpha_i}(\tau) = \lim_{T\to\infty} \frac{1}{T} \sum_{t=0}^{T-1} (s_i(t) s_i(t) s_i(t) s_i(t+\tau)) e^{-j8\pi\alpha_i t}, \tag{24}$$

$$M_{2s_i}^{\alpha_i}(\tau) = \lim_{T\to\infty} \frac{1}{T} \sum_{t=0}^{T-1} (s_i(t) s_i(t+\tau)) e^{-j4\pi\alpha_i t}, \tag{25}$$

and T is the finite time. Also, $C_{x_i x_i x_i y}^{\alpha_i - f}(\tau)$ can be expressed as

$$\begin{aligned} C_{x_i x_i x_i y}^{\alpha_i - f}(\tau) = {} & r_i^3 r'_i e^{-j\pi f_{d_i} \tau} e^{-j\pi(\alpha_i - f + f_{d_i}) D_i} \\ & \cdot e^{-j\pi(\alpha_i - f + f_{d_i}) D_i} M_{s_i s_i n s_i}^{\alpha_i - f + f_{d_i}}(\tau - D_i) \\ & - 3B r_i r'_i e^{-j\pi f_{d_i} \tau} e^{-j\pi(\alpha_i - f + f_{d_i}) D_i} \\ & \cdot R_{s_i}^{\alpha_i - f + f_{d_i}}(\tau - D_i) + r_i^3 M_{s_i s_i n' s_i}^{\alpha_i - f + f_{d_i}}(\tau - D_i), \end{aligned} \tag{26}$$

where $B = E[x_i(t)y(t)]$, $R_{s_i}^{\alpha_i - f + f_{d_i}}(\tau - D_i)$ is the cyclic self-correlation of $s_i(t)$, given by

$$R_{s_i}^{\alpha_i - f + f_{d_i}}(\tau) = \lim_{T\to\infty} \frac{1}{T} \sum_{t=0}^{T-1} (s_i(t)s_i(t+\tau))e^{-j2\pi\alpha_i t}. \tag{27}$$

In addition, $M_{s_i s_i n s_i}^{\alpha_i - f + f_{d_i}}(\tau - D_i)$ is the fourth-order cross-cyclic cumulant between $s_i(t)$ and the noise in the reference channel, $M_{s_i s_i n' s_i}^{\alpha_i - f}(\tau)$ is the fourth-order cross-cyclic cumulant between $s_i(t)$ and the noise in the surveillance channel, given by

$$\begin{aligned} M_{s_i s_i n s_i}^{\alpha_i - f + f_{d_i}}(\tau - D_i) = \lim_{T\to\infty} \frac{1}{T} \sum_{t=0}^{T-1} (s_i(t)s_i(t)n(t)) \\ \cdot s_i(t+\tau-D_i)e^{-j2\pi(\alpha_i - f + f_{d_i})t}, \end{aligned} \tag{28}$$

and

$$\begin{aligned} M_{s_i s_i n' s_i}^{\alpha_i - f + f_{d_i}}(\tau - D_i) = \lim_{T\to\infty} \frac{1}{T} \sum_{t=0}^{T-1} (s_i(t)s_i(t)n'(t)) \\ \cdot s_i(t+\tau-D_i)e^{-j2\pi(\alpha_i - f + f_{d_i})t}. \end{aligned} \tag{29}$$

2) Four-Weighted Fractional Fourier Transform Fourth-Order Cyclic Cumulant Cross Ambiguity Function: Fractional Fourier transform (FRFT) can show signals in the fractional domain between the time domain and the frequency domain, which can be defined as [20]

$$F_\beta(u) = F_\beta\left[f(t)\right](u) = \int_{-\infty}^{\infty} f(t)\kappa_\beta(u,t)dt, \tag{30}$$

where F_β denotes the FRFT operators, the relationship between the order p and the angle β of FRFT is $\beta = \frac{\pi}{2}p$, $\kappa(u,t)$ is the integral kernel and it is the continuous function of p, which can be expressed as [21]-[22]

$$\begin{aligned} \kappa(u,t) &= \sum\nolimits_{n=0}^{+\infty} e^{-jn\beta} H_n^*(t)H_n(u), \\ &= \begin{cases} A_\beta e^{\frac{j}{2}(t^2+u^2)\cot\beta - jtu\csc\beta} & \beta \neq k\pi, \\ \delta(t-u) & \beta = 2k\pi, \\ \delta(t+u) & \beta = (2k-1)\pi, \end{cases} \end{aligned} \tag{31}$$

where k is an integer and $A_\beta = \sqrt{(1 - j\cot\beta)/2\pi}$. The transformation relationships of coordinates can be given by

$$\begin{bmatrix} t \\ \omega \end{bmatrix} = \begin{bmatrix} \cos\beta & \sin\beta \\ -\sin\beta & \cos\beta \end{bmatrix} \begin{bmatrix} u \\ f \end{bmatrix} = \begin{bmatrix} u\cos\beta + f\sin\beta \\ -u\sin\beta + f\cos\beta \end{bmatrix}, \tag{32}$$

and

$$\begin{bmatrix} u \\ f \end{bmatrix} = \begin{bmatrix} t\cos\beta - \omega\sin\beta \\ t\sin\beta + \omega\cos\beta \end{bmatrix}. \tag{33}$$

There are no cross terms because FRFT is a linear transformation, which is beneficial to effectively separate signal form interference or noise. From the properties of Fourier transform (FT), we can obtain the four-weighted fractional Fourier transform (FWFRFT) as [23]

$$\begin{aligned} F_{4w}^\beta[g(x)] = \omega_0(\beta)g_0(x) + \omega_1(\beta)g_1(x) \\ + \omega_2(\beta)g_2(x) + \omega_3(\beta)g_3(x), \end{aligned} \tag{34}$$

where p is the order of FWFRFT, $g_0(x)-g_3(x)$ denote the 0-3 times FT of $g(x)$, the weighting factor $\omega_0(\beta)-\omega_3(\beta)$ can be expressed as

$$\omega_l(\beta) = \cos\left[\frac{(p-l)\pi}{4}\right]\cos\left[\frac{2(p-l)\pi}{4}\right]\exp\left[\frac{3(p-l)\pi}{4}\right], \tag{35}$$

where $l = 0, 1, 2, 3$. From (31), the FRFT of the ambiguity function is equivalent to its rotation by β degrees into fractional domain, that is

$$AF_\beta(t,w) = AF(t\cos\beta - \omega\sin\beta, t\sin\beta + \omega\cos\beta). \tag{36}$$

When $AF(u,f) = \chi_{y,x_i}^{\alpha_i - f, \alpha_i}(u,f)$ and $\beta = 0, \frac{\pi}{2}, \pi, \frac{3\pi}{2}$, we can get the 0th to 3rd order FT of the ambiguity function $AF_\beta^{(0)}(t,\omega)$, $AF_\beta^{(1)}(t,\omega)$, $AF_\beta^{(2)}(t,\omega)$ and $AF_\beta^{(3)}(t,\omega)$. The weighting factors will be determined as long as β is determined. The four-weighted fractional Fourier transform fourth-order cyclic cumulant cross ambiguity function (FWFRFT-FOCCCAF) can be obtained by

$$\begin{aligned} F_{4w}^\beta(t,\omega) = \omega_0(\beta)AF_\beta^{(0)}(t,\omega) + \omega_1(\beta)AF_\beta^{(1)}(t,\omega) \\ + \omega_2(\beta)AF_\beta^{(2)}(t,\omega) + \omega_3(\beta)AF_\beta^{(3)}(t,\omega). \end{aligned} \tag{37}$$

3) Feature extraction: We can obtain the abscissas $D_{\max}$ and $f_{d\max}$ by using appropriate peak extraction to search from the two two-dimensional sections on the time axis and the frequency axis, and the combination of the two abscissas is the coordinate for the peak of the three-dimensional graph of FWFRFT-FOCCCAF, and it contains the information of TDOA and FDOA. This is formulated as

$$(D_{\max}, f_{d\max}) = \arg\max\left[F_{4w}^\beta(t,\omega)\right]. \tag{38}$$

We can calculate the TDOA and FDOA accordingly as

$$\begin{cases} D = \frac{N'}{2f_s} - 2D_{\max}, \\ \\ f_d = \frac{N'}{2f_s} - 4f_c + f_{d\max}, \end{cases} \tag{39}$$

where N' is the length, f_s is the sampling frequency, and f_c denotes the carrier frequency of the signal.

The direct wave signal and echo signal show a strong correlation when the time and frequency parameters equal TDOA and FDOA, and the amplitude of the FWFRFT-FOCCCAF peaks in the two two-dimensional sections. The following spectral peak extraction method can extract the coordinates $\tau_{\max}$ and $f_{d\max}$ from the peaks accurately and effectively:

i) Put the data of two-dimensional section into the array W, and mark an ith element as w_i;

ii) Obtain a new array W' through the backward differential processing of W. The jth element of W', w_{j}' can be obtained by

$$w_{\mathrm{j}}' = w_j - w_{j-1}. \tag{40}$$

Let $w_{\mathrm{j}}' = 0$ when $w_{\mathrm{j}}' < 0$. The mutation at the spectral peak is stored in the array as a maximum after the backward differential operation;

iii) The array element of W', which is greater than zero, is

$$ave = \frac{1}{n}\sum\nolimits_{i=1}^{n} w'_j, \tag{41}$$

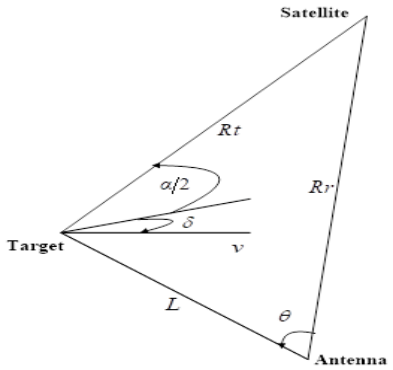

Fig. 2. Geometrical structure of the velocity and distance.

$$w'_j = \begin{cases} w'_j - \frac{(ave)^2}{w'_j} & w'_j > 0, \\ 0 & w'_j \le 0, \end{cases} \tag{42}$$

where n is the number of elements that are greater than zero in the array. (41) finds the mean of all array elements greater than zero and all the elements of the array are reduced by the subtraction operation in (42). Because the array elements that contain spectral peaks are the maximum values, they are almost unchanged after the subtraction in (42).

iv) Calculate the sum and average of the array obtained in iii) and set the array element less than the average to zero.

v) Do the loop operation on iv) until the sum of the array equals to one of the elements w''_k exactly, the subscript of which is the abscissa of spectral peak of two-dimensional sections.

C. Velocity and Distance Estimation

The moving aerial target has the same velocity and the same distance between the target and the receiver from different satellites. Therefore, the TF-LV transform of different TDOA-FDOA spectrum is used to unify the distance and velocity of the target form different satellite signals. The geometrical structure of the velocity and distance is shown in Fig. 2, where L denotes the distance from the target to the receiver, α stands for the bi-static angle and δ represents the angle between bi-static angle bisector and the velocity v of the target. Therefore, the TF-LV transform of different TDOA-FDOA spectrum is used. The relationship between the TDOA and the distance is

$$\begin{cases} L + R_t = R_r + cD, \\ R_t^2 = R_r^2 + L^2 - 2R_r L\cos\theta, \end{cases} \tag{43}$$

where L is the distance from the target to the receiver, α stands for the bistatic angle and δ is the angle between bistatic angle bisector and the velocity v of the target. We can obtain

$$L = \frac{c^2D^2 + 2R_rcD}{2(R_r + cD - R_r\cos\theta)} = f(D), \tag{44}$$

$$R_t = \frac{R_r(R_r - R_r\cos\theta + cD - cD\cos\theta) + \frac{1}{2}c^2D^2}{R_r + cD - R_r\cos\theta}. \tag{45}$$

The relationship between f_d and v is

$$f_d = \frac{2v}{\lambda}\cos\delta\cos\frac{\alpha}{2} \approx \frac{2v}{\lambda}\cos\frac{\alpha}{2} = g(v), \tag{46}$$

$$v = \frac{f_d\lambda}{2\cos\frac{\alpha}{2}}, \tag{47}$$

where $\lambda = 1/f_c$, f_c is the frequency of the signal, and α can be obtained as

$$\cos\alpha = \frac{{R_t}^2 + L^2 - {R_r}^2}{2R_tL}. \tag{48}$$

The data weighted fusion method based on the minimum overall variance is used to fuse multiple pairs of L and v after the TF-LV transformation. A weighting factor is assigned to each data so that the overall variance reaches the minimum. Finally, global estimation is obtained by the local estimation and weighting factor. The process of the fusion is described as follows.

Assuming that the weighting factor of L_i is $w_i (i = 1, 2, \ldots, M')$, the overall estimate $\hat{L}$ after fusing is [22]

$$\begin{cases} \hat{L} = \sum_{i=1}^{M'} w_i L_i, \\ \sum_{i=1}^{M'} w_i = 1. \end{cases} \tag{49}$$

We can get the overall variance for the TDOA estimation from (49) as

$$\begin{aligned} \sigma_L^2 &= E\left[\left(L - \hat{L}\right)^2\right] = E\left[\left(\sum_{i=1}^{M'} w_i L - \sum_{i=1}^{M'} w_i L_i\right)^2\right] \\ &= E\left[\left(\sum_{i=1}^{M'} w_i \left(L - L_i\right)\right)^2\right] \\ &= E\left[\sum_{i=1}^{M'} w_i^2 (L - L_i)^2 + \sum_{\substack{i,j=1 \\ i\neq j}}^{M'} w_i w_j \left(L - L_i\right)\left(L - L_j\right)\right]. \end{aligned} \tag{50}$$

Because L_i and L_j are independent of each other when $i \neq j$, one has

$$\sum_{\substack{i,j=1 \\ i\neq j}}^{M'} w_i w_j \left(L - L_i\right)\left(L - L_j\right) = 0, \tag{51}$$

and (50) can be further written as:

$$\sigma_L^2 = E\left[\sum_{i=1}^{M'} w_i^2 (L - L_i)^2\right] = \sum_{i=1}^{M'} w_i^2 P_i, \tag{52}$$

where $P_i = E\left[(L - L_i)^2\right]$ is the variance of each estimate. It can be seen from (52) that σ_L^2 is a multivariable quadratic function of random weighting factors $w_i (i = 1, 2, ..., M')$. According to the multivariate extreme value theory, the minimum of σ_L^2 exists and is given as

$$\sigma_{L_{\min}}^2 = \min\left(\sum_{i=1}^{M'} w_i^2 P_i\right). \tag{53}$$

By solving (53), the optimal random weighting factor when

the overall variance is minimum is

$$w_i^* = \frac{1}{P_i \sum_{i=1}^{M'} \frac{1}{P_i}}. \tag{54}$$

Therefore, the minimum of the overall variance is

$$\sigma^2_{L_{\min}} = \frac{1}{\sum_{i=1}^{M'} \frac{1}{P_i}}. \tag{55}$$

We can get the final distance $\hat{L}$ through (49) after the fusion of $L_i (i = 1, 2, ..., M')$ with the weighting factor getting by (54). The process for the fusion of $\hat{v}$ is the same as $\hat{L}$.

IV. CRLBs of Location Parameters Estimators

Cramer-Rao Lower Bound (CRLB) is one of the criteria for analyzing the effectiveness of estimation [24]. The CRLBs of the estimated location parameters will be deduced in this section. Let $y(t)$ represent the signal in the surveillance channel after the DPI and MPI suppression. $y(t)$ only contains the weak echo signal and complex zero-mean white Gaussian noise as

$$y(t) = \sum\nolimits_{\eta=1}^{M'} r'_\eta s_\eta(t - D_\eta) e^{-j2\pi f_{d_\eta} t} + n'(t), \tag{56}$$

and the energy of the η_{th} weak echo signal without noise is

$$E_\eta = (r'_\eta)^2 \int_{-\infty}^{\infty} |s_\eta(t)|^2 dt, \tag{57}$$

and the power spectral density of the noise satisfies

$$E\{n(t)n(t')\} = 0, \tag{58}$$

$$E\{n(t)n^*(t')\} = N_0 \delta(t - t'), \tag{59}$$

where N_0 is the power spectral density of the noise, $E\{\cdot\}$ is the expectation operator, superscript stands for the complex conjugate of a signal, and $\delta\{\cdot\}$ denotes the Dirac delta function.

The estimated vector consisting of TDOA and FDOA is given by

$$\theta = [D_1 \quad D_2 \dots D_{M'} \quad f_{d_1} \quad f_{d_2} \dots f_{d_{M'}}]^T. \tag{60}$$

The probability density function (P.D.F.) of the echo signal can be expressed as

$$\begin{aligned} p(y;\theta) = K \exp\Bigg\{ & -\frac{1}{N_0} \int_{-\infty}^{\infty} \\ & \cdot \Big| y(t) - \sum_{\eta=1}^{M'} r'_\eta s_\eta(t - D_\eta)\ e^{-j2\pi f_{d_\eta} t} \Big|^2 dt \Bigg\}, \end{aligned} \tag{61}$$

where $K = 1/\sqrt{2\pi}$. The log-likelihood function is

$$\begin{aligned} \ln p(y;\theta) = & -\frac{1}{N_0} \int_{-\infty}^{\infty} |y(t) \\ & - \sum_{\eta=1}^{M'} r'_\eta s_\eta(t - D_\eta) e^{-j2\pi f_{d_\eta} t}|^2 dt + \ln K. \end{aligned} \tag{62}$$

Thus,

$$\frac{\partial \ln p(y,\theta)}{\partial D_\eta} = -\frac{2r'_\eta}{N_0} \mathrm{Re} \int_{-\infty}^{\infty} n'(t) \dot{s}^*_\eta(t - D_\eta) e^{j2\pi f_{d_\eta} t} dt, \tag{63}$$

$$\frac{\partial \ln p(y,\theta)}{\partial f_{d_\eta}} = -\frac{4\pi r'_\eta}{N_0} \mathrm{Im} \int_{-\infty}^{\infty} t\, n'(t) s^*_\eta(t - D_\eta) e^{j2\pi f_{d_\eta} t} dt, \tag{64}$$

where $\eta, \eta' = 1, 2, \dots, M'$, $\dot{s}(t) = \frac{ds(t)}{dt}$, $\mathrm{Re}\{\cdot\}$ and $\mathrm{Im}\{\cdot\}$ denote the real part and imaginary part of a function, respectively.

It is well known that the CRLB of any unbiased estimator $\hat{\theta}_i$ must satisfy

$$\mathrm{var}(\hat{\theta}_i) \geq \left[I^{-1}(\theta)\right]_{i,i}, \tag{65}$$

where $\left[I^{-1}(\theta)\right]_{i,i}$ denotes the $[i,i]th$ element of the inverse of the Fisher Information Matrix (FIM) is defined by

$$[I(\theta)]_{i,i} = I_{i,j} = E\left\{ \frac{\partial \ln p(y;\theta)}{\partial \theta_i} \frac{\partial \ln p(y;\theta)}{\partial \theta_j} \right\}. \tag{66}$$

For convenience, define

$$SNR_\eta = \frac{E_\eta}{N_0} \tag{67}$$

$$P_\eta = \frac{(r'_\eta)^2}{E_\eta} \int_{-\infty}^{\infty} t |s_\eta(t)|^2 dt \tag{68}$$

$$G_\eta = \frac{(r'_\eta)^2}{E_\eta} \int_{-\infty}^{\infty} t^2 |s_\eta(t)|^2 dt \tag{69}$$

$$H_\eta = \frac{(r'_\eta)^2}{E_\eta} \mathrm{Im} \int_{-\infty}^{\infty} s^*_\eta(t) \dot{s}_\eta(t) dt \tag{70}$$

$$L_\eta = \frac{(r'_\eta)^2}{E_\eta} \int_{-\infty}^{\infty} |\dot{s}_\eta(t)|^2 dt \tag{71}$$

$$Q_\eta = \frac{(r'_\eta)^2}{E_\eta} \mathrm{Im} \int_{-\infty}^{\infty} t s^*_\eta(t) \dot{s}_\eta(t) dt \tag{72}$$

These symbols have physical meanings and can also be expressed in the frequency domain, where (68) stands for SNR, (68)-(72) are the waveform parameters of the weak echo signal described in [25]-[26]. Thus,

$$\begin{aligned} I_{\eta\eta} &= \frac{\partial^2 \ln p(y,\theta)}{\partial D_\eta^2} \\ &= \frac{2(r'_\eta)^2}{N_0} \mathrm{Re} \int_{-\infty}^{\infty} |\dot{s}_\eta(t - D_\eta)|^2 dt \\ &= 2SNR_\eta L_\eta = 2SNR_\eta A_\eta, \end{aligned} \tag{73}$$

$$\begin{aligned} I_{\eta,\eta+M'} = I_{\eta+M',\eta} &= \frac{\partial^2 \ln p(y,\theta)}{\partial D_\eta \partial f_{d_\eta}} \\ &= \frac{4\pi (r'_\eta)^2}{N_0} \mathrm{Im} \int_{-\infty}^{\infty} t \dot{s}_\eta(t - D_\eta) s^*_\eta(t - D_\eta) dt \\ &= 4\pi SNR_\eta (Q_\eta + H_\eta D_\eta) = 2SNR_\eta 2\pi B_\eta, \end{aligned} \tag{74}$$

$$
\begin{aligned}
I_{\eta+M',\eta+M'} &= \frac{\partial^2 \ln p(y,\theta)}{\partial f_{d_\eta}^2} \\
&= \frac{8\pi^2 (r'\eta)^2}{N_0} \mathrm{Re} \int_{-\infty}^{\infty} t^2 s_\eta^*(t-D_\eta) s_\eta(t-D_\eta) dt \quad (75) \\
&= 8\pi^2 SNR_\eta [G_\eta + 2P_\eta D\eta - D_\eta^2 E_\eta] \\
&= 2SNR_\eta 4\pi^2 C_\eta,
\end{aligned}
$$

$$
I_{other} = \frac{\partial^2 \ln p(y,\theta)}{\partial D_\eta \partial D_{\eta'}} = \frac{\partial^2 \ln p(y,\theta)}{\partial D_\eta \partial f_{d_{\eta'}}} = \frac{\partial^2 \ln p(y,\theta)}{\partial f_{d_\eta} \partial f_{d_{\eta'}}} = 0, \quad (76)
$$

where $\eta, \eta' = 1, 2, \ldots, M'$, $\eta \neq \eta'$. And A_η, B_η and C_η are defined as

$$
A_\eta = L_\eta, \quad (77)
$$

$$
B_\eta = Q_\eta + H_\eta D_\eta, \quad (78)
$$

$$
C_\eta = G_\eta + 2P_\eta D_\eta - D_\eta^2 E_\eta. \quad (79)
$$

Therefore, the FIM can be expressed as

$$
I(\theta) = 2SNR \begin{bmatrix}
A_1 & & & 2\pi B_1 & & \\
& \ddots & & & \ddots & \\
& & A_{M'} & & & 2\pi B_{M'} \\
2\pi B_1 & & & 4\pi^2 C_1 & & \\
& \ddots & & & \ddots & \\
& & 2\pi B_{M'} & & & 4\pi^2 C_{M'}.
\end{bmatrix} \quad (80)
$$

Taking the inverse of FIM, we can obtain the CRLBs of joint TDOA and FDOA estimation of the ηth weak echo signal as

$$
Var(\hat{D}_\eta)_{CRLB} = \frac{1}{2SNR_\eta} \cdot \frac{C_\eta}{A_\eta C_\eta - B_\eta^2}, \quad (81)
$$

$$
Var(\hat{f}_{d_\eta})_{CRLB} = \frac{1}{8\pi^2 SNR_\eta} \cdot \frac{A_\eta}{A_\eta C_\eta - B_\eta^2}. \quad (82)
$$

From (81) and (82), we can see that the CRLBs of the joint estimation of TDOA and FDOA for the ηth weak echo signal are related to SNR and waveform parameters A_η, B_η and C_η, which are determined when the satellite type is determined.

The relationship between the TDOA of the weak echo signal and the distance from the target to the receiver is $L_\eta = R_r - R_t + cD_\eta$, $\eta = 1, 2, ..., M'$, and R_r and R_t are constants. However, D_η may affect the accuracy of the estimation because D_η is also a variable needs to be estimated. According to the definition of the CRLB for the non-random parameter function, we can obtain the CRLB of the ηth distance estimate as

$$
Var(\hat{L}_\eta)_{CRLB} = c^2 Var(\hat{D}_\eta)_{CRLB}, \quad (83)
$$

where $\eta = 1, 2, \ldots, M'$. From the weighted data fusion algorithm, we obtain the CRLB of $\hat{L}$ as

$$
Var(\hat{L})_{CRLB} = \frac{1}{\sum_{\eta=1}^{M'} \frac{1}{Var(\hat{L}_\eta)_{CRLB}}} = \frac{c^2}{\sum_{\eta=1}^{M'} \frac{1}{Var(\hat{D}_\eta)_{CRLB}}}, \quad (84)
$$

The relationship between the FDOA of the weak echo signal and the velocity of the target is $v_\eta = \frac{f_{d_\eta} \lambda}{2 \cos \frac{\beta_\eta}{2}}$, $\eta = 1, 2, \ldots, M'$, where β_η is the bistatic angle. Therefore, v_η is a function of the FDOA and can be further written as $v_\eta = U_\eta f_{d_\eta}$ when $U_\eta = \frac{\lambda}{2 \cos \frac{\beta_\eta}{2}}$, where f_{d_η} is also a variable and will affect the accuracy of the estimation of velocity. According to the definition of the CRLB for the non-random parameter function, we can obtain the CRLB of velocity estimate for the ηth weak echo signal as

$$
Var(\hat{v}_\eta)_{CRLB} = U_\eta^2 \, Var(\hat{f}_{d_\eta})_{CRLB}, \quad (85)
$$

where $\eta = 1, 2, \ldots, M'$. From the weighted data fusion algorithm, we can obtain the CRLB of $\hat{v}$ as

$$
Var(\hat{v})_{CRLB} = \frac{1}{\sum_{\eta=1}^{M'} \frac{1}{Var(\hat{v}_\eta)_{CRLB}}} = \frac{1}{\sum_{\eta=1}^{M'} \frac{1}{U_\eta^2 \, Var(\hat{f}_{d_\eta})_{CRLB}}}. \quad (86)
$$

V. Numerical Results and Discussion

Simulation results are presented in this section. The simulation setups are described as follows. The satellite models are GPS, DVB-S and INMARSAT. Their carrier frequencies are 1575.42MHz, 12.38GHz and 1640MHz, respectively. Their symbol rates are 1.023MHz, and 22.425MHz, 2.2MHz [27]. The TDOA are $25\mu s$, $16\mu s$ and $10\mu s$, and the FDOA are 17640Hz, 14480Hz and 11080Hz, respectively. The velocity of the target is set to 350 m/s. the distance between the target and the receiver is 20 km and the angle of FWFRFT is $\pi/4$. The number of sampling points is 10^7 and additive complex white Gaussian noise (AWGN) is adopted. The SNRs of echo signals are set to -112 dBm. In addition, we use 2000 Monte Carlo experiments for every scene. The normalized mean square error (NMSE) is adopted as the performance measure with [25]

$$
NMSE = \frac{|\hat{\rho} - \rho|^2}{\rho^2}, \quad (87)
$$

where ρ is the theoretical value and $\hat{\rho}$ is the estimated value of the parameter. The normalized CRLB is defined as:

$$
Var(\hat{\rho})_{NCRLB} == \frac{Var(\hat{\rho})_{CRLB}}{\rho^2}, \quad (88)
$$

where $Var(\hat{\rho})_{CRLB}$ is the CRLB of the estimated parameter.

A. Location Parameter Estimation Performance with Different SNRs

To reveal the effect of the echo SNR on the location parameter estimation performance, the performances of the two proposed parameter estimation methods are simulated for different SNRs ranging from -80dB to -10dB. Fig. 3 and Fig. 4 show the estimation performance of TDOA and the distance between the target and receiver, respectively. It can be seen from Fig. 3 that the three satellite signals can be used to estimate the TDOA of weak echo signals. Besides, the TDOA estimation performance is improved and close to the NCRLB when the SNR increases. The NMSEs of TDOA estimation for GPS, DVB-S and INMARSAT echo signals reach 10^{-3} when the SNR is -45dB, -40dB and -30dB, respectively, indicating that the TDOA estimation performance based on the GPS is

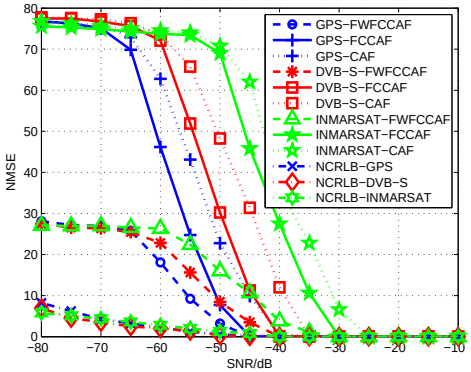

Fig. 3. TDOA estimation performance with different SNRs.

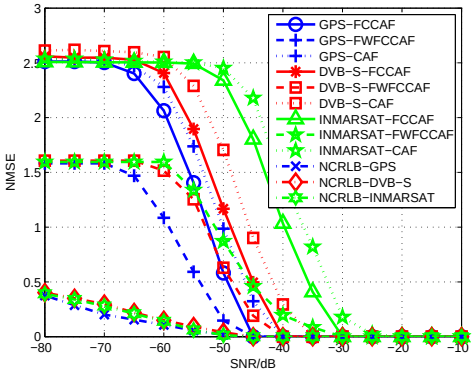

Fig. 5. FDOA estimation performance with different SNRs.

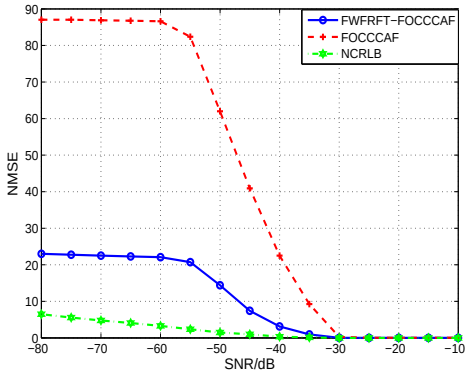

Fig. 4. Distance estimation performance with different SNRs.

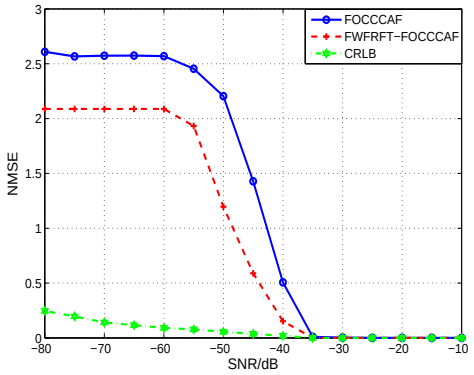

Fig. 6. Velocity estimation performance with different SNRs.

the best, while that based on the INMARSAT is the worst. Fig. 4 illustrates that the three satellite signals can be used to estimate the distance between the target and the receiver when the SNR is large. Fig. 5 shows that the three satellite signals can be used to estimate the FDOA of the weak echo signal, and the FDOA estimation performance of the three satellites weak echo signals are improved and close to the NCRLB with the increase of SNR. From Fig. 6, we can observe that the NMSE of velocity estimation for the target reaches to 10^{-3} when the SNR is -35dB. Moreover, the CAF and FOCCCAF yield higher NMSE than the FWFRFT-FOCCCAF TDOA and FDOA estimation method, implying that the CAF and FOCCCAF have worse location parameter estimation performance and the FWFRFT has better suppression of interference and noise.

B. Location Parameter Estimation Performance with Different Numbers of Coherent Cumulative Points of Signals

To investigate the impact of the number of coherent cumulative points of the signal on the location parameter estimation performance, simulations are conducted under the signal sampling points number of 10^6, 10^7 and 10^8. The GPS signal is adopted to estimate the TODA and FDOA, and the GPS, DVB-S and INMARSAT are used to estimate the distance and velocity. Fig. 7 and Fig. 8 show the estimation performance of the TDOA and the distance between a target and a receiver. Fig. 9 and Fig. 10 depict the estimation performance of FDOA and the velocity of the target. From Fig. 7, it is easy to see that the TDOA estimation performance improves when the number of coherent points increases. Furthermore, the NMSE of TDOA for GPS reaches 10^{-3} when the SNR is -35dB and the number of signal point is 10^6. Moreover, the performance is improved by 10 dB when the number increases by an order of magnitude. This is because the spectral peak becomes more prominent with the increase of the number of cumulative points, equivalent to improve the gain of SNR. As a result, it can improve the TDOA estimation performance. Fig. 8 shows that the distance estimation performance improves with the increase of the number of coherent points. The NMSEs of distance estimate become 10^{-3} under the SNR of -15dB, -30dB, -40dB and the number of point of 10^6, 10^7 and 10^8, respectively. As the accuracy of the distance estimate depends on the performance of TDOA estimations, an accurate TDOA estimation with the increasing number of points results in an accurate estimation of the distance between a target and a receiver. It can be seen from Fig. 9 that with the increase of the number of points, the FDOA estimation performance is improved, and the NMSE of FDOA estimation reaches to 10^{-3} when the SNR is -35dB and the number of point is 10^6. Moreover, the performance is improved by 10 dB when the number of signal cumulative points increases by an order of magnitude. The reason behind this phenomenon is that the spectral peak becomes more prominent with the increase of the number of cumulative points. It is also equiv-

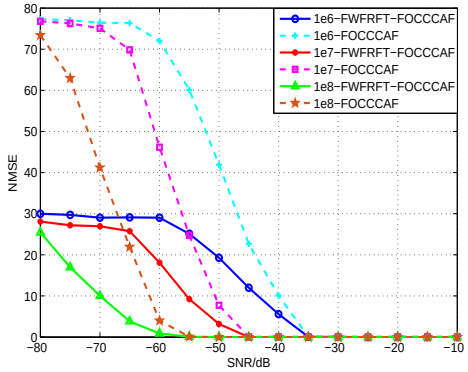

Fig. 7. TDOA estimation performance with different coherent cumulative points of the signals.

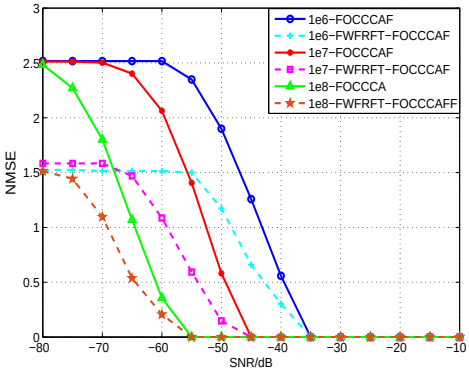

Fig. 9. FDOA estimation performance with different coherent cumulative points of the signals.

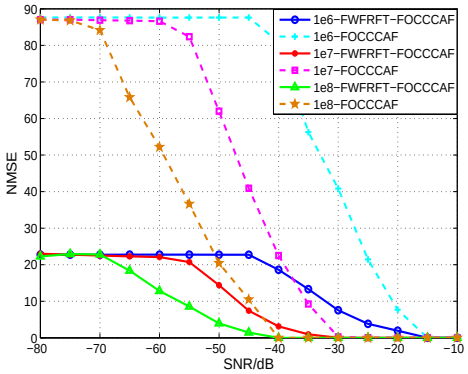

Fig. 8. Distance estimation performance with different coherent cumulative points of the signals.

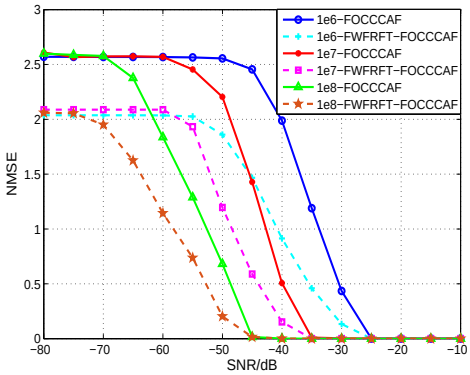

Fig. 10. Velocity estimation performance with different coherent cumulative points of the signals.

alent to improving the gain of SNR, so that it can improve the FDOA estimation performance. Fig. 10 shows that the velocity estimation performance improves with the increase of the number of coherent points, and the NMSE of FDOA estimation becomes 10^{-3} when the SNR is -25 dB and the number of point is 10^6. Beside, the performance is improved by 10 dB when the number increases by an order of magnitude. This is because the accuracy of velocity estimation depends on the performance of FDOA estimation and the increase of points leads to more accurate FDOA estimation and velocity estimation.

C. Location Parameter Estimation Performance with Different SDRs

Fig. 11-Fig. 14 present the location parameter estimation performance versus different signal-to-direct signal-ratio (SDR). From Fig. 11, it can be observed that the TDOA estimation performance improves with the increase of SDR under the same SNR. Besides, the estimation performance increases by 5dB when SDR increases by 20dB, as it is equivalent to enhance the power of echo signal and make the spectrum peak more prominent when the direct wave power is fixed. Therefore, it can improve the performance of TDOA estimation through increasing the SDR. Fig. 12 shows that the distance estimation performance is improved with the increase of SDR, and the NMSE of distance estimation reach to 10^{-3} when the SNR is -20dB and the SDR is -40dB, and the distance estimation performance increases by 5dB when SDR adds by 20dB similarly. Because the accuracy of the distance estimation depends on the performance of the TDOA estimation. The TDOA estimation is more accurate when SDR increases, so the distance estimation becomes more accurate. It can be seen from Fig. 13 that the FDOA estimation performance of the weak echo signal becomes better with the increase of SDR, and the NMSE of FDOA estimation reach 10^{-3} when the SNR is -35dB and the SDR is -40dB. The estimation performance increases by 5dB when SDR increases by 20dB. Therefore, there is a better FDOA estimation performance. Fig. 14 shows that the velocity estimation performance is improved with the increase of SDR, and the NMSE of FDOA estimation reach 10^{-3} when the SNR is -25dB and the SDR is -40dB. Besides, the estimation performance increases by 5dB when SDR adds by 20dB. Because the accuracy of the velocity estimation depends on the performance of the FDOA estimation. The FDOA estimation is more accurate with the increase of SDR, so the velocity estimation becomes more accurate. Moreover, the FOCCCAF has a higher NMSE than that of the FWFRFT-FOCCCAF method, indicating that the FWFRFT has a better effect on the suppression of interference and noise.

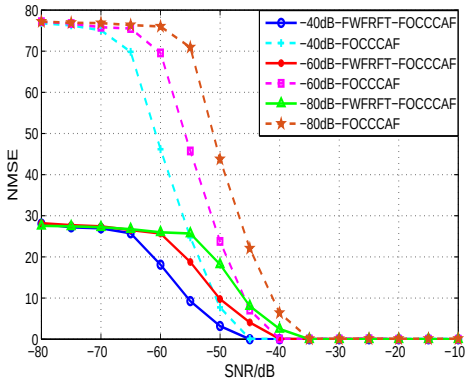

Fig. 11. TDOA estimation performance with different SDRs.

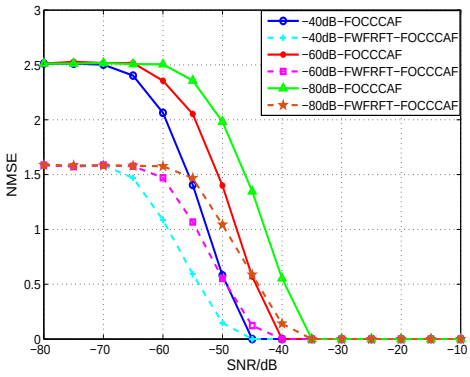

Fig. 13. FDOA estimation performance with different SDRs.

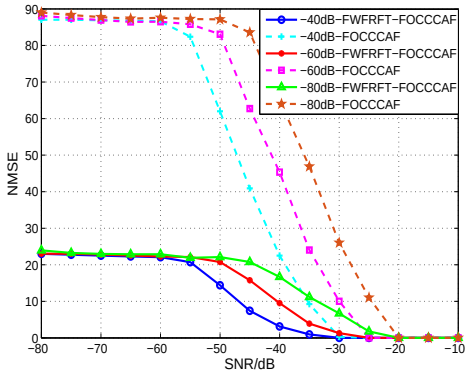

Fig. 12. Distance estimation performance with different SDRs.

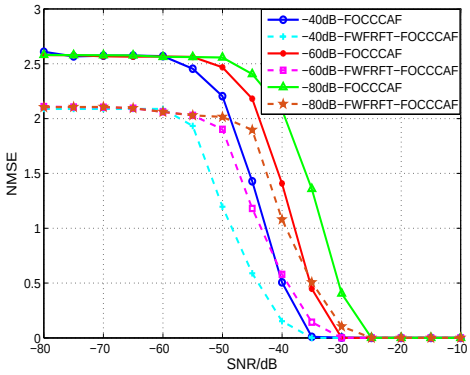

Fig. 14. Velocity estimation performance with different SDRs.

D. Location Parameters Estimation Performance with Different Number of Satellites

Fig. 15 and Fig. 16 show the the distance and velocity estimation performance under the different number of satellites, respectively. From Fig. 15, we can see that the NMSEs of distance estimation reach to 10^{-3} when the SNR are -32dB, -30dB and -28dB and the number of satellite is 2, 3 and 4, respectively. This indicates that the distance estimation becomes worse when the number of satellite increases, since the increase of satellites leads to the increase of DPI and MPI in the surveillance channel. However, the increasing number of satellites will improve the reliability of parameter estimation. From Fig. 16, the NMSEs of distance estimation reach 10^{-3} when the SNR are -36dB, -34dB and -32dB and the number of satellite is 2, 3 and 4. The performance of velocity estimations gradually decreases with the increasing number of satellites, while the reliability gradually improves, which is consistent with distance estimation.

VI. Conclusion

In order to enhance the accuracy and reliability of moving aerial target location parameter estimation, a novel framework of the passive location system in space-air-ground integrated networks-based internet of vehicles has been designed and corresponding location parameter estimation method based on FOCCCAF and FWFRFT-FOCCCAF has been proposed in this paper. Simulation results shown that the proposed method has estimated effectively the location parameters of moving aerial target and FWFRFT-FOCCCAF outperforms FOCCCAF on location parameter estimations. Moreover, the performance of proposed method improves by increasing the SNR of the echo signal, the coherent cumulative points of the signals and the SDR between the direct wave and the echo signal, while increasing the number of satellites does not improve the estimation performance but can improve the estimation reliability.

References

[1] T. Yang, H. Feng, C. Yang, Y. Wang, J. Dong, M. Xia,"Multivessel computation offloading in maritime mobile edge computing network," *IEEE Internet of Things Journal*, vol. 6, no. 3, pp. 4063-4073, June 2019.

[2] T. Yang, H. Feng, S. Gao, Z. Jiang, M. Qin, N. Cheng, L. Bai, "Two-stage offloading optimization for energy-latency tradeoff with mobile edge computing in maritime networks," *IEEE Internet of Things Journal*, vol. 7, no. 7, pp. 5954-5963, July 2020.

[3] Y. Wang, Q. Li, J. Jiao, S. Wu, and Q. Zhang, "ARM: adaptive random-selected multi-beamforming estimation scheme for satellite-based internet of things," *IEEE Access*, vol. 7, pp. 63264-63276, May 2019.

[4] D. Hu, L. He, and J. Wu, "A novel forward-link multiplexed scheme in satellite-based internet of things," *IEEE Internet of Things Journal*, vol. 5, no. 2, pp. 1265-1274, Apr. 2018.

[5] M. Liu, K. Yang, N. Zhao, Y. Chen, H. Song, F. Gong, "Intelligent signal classification in industrial distributed wireless sensor networks-based IIoT," *IEEE Transactions on Industrial Informatics*, 2020. DOI: 10.1109/TII.2020.3016958.

[6] M. Liu, G. Liao, N. Zhao, H. Song and F. Gong. "Data-driven deep learning for dignal classification in industrial cognitive radio networks," *IEEE Transactions on Industrial Informatics*, vol. 17, no. 5, pp. 3412-3421, May. 2021.

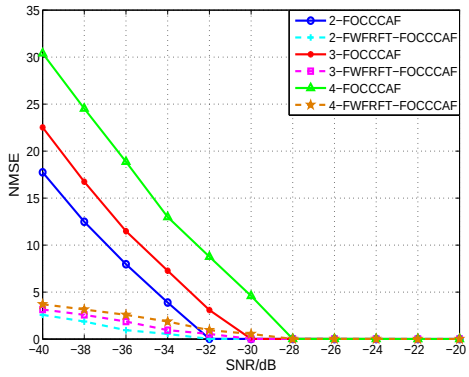

Fig. 15. Distance estimation performance with different number of satellites.

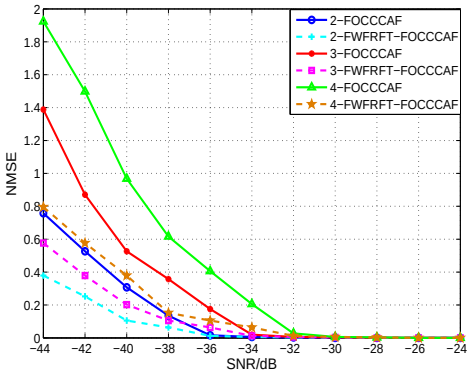

Fig. 16. Velocity estimation performance with different number of satellites.

[7] T. Yang, H. Liang, N. Cheng and X. Shen, "Efficient scheduling for video transmission in maritime wireless communication network," *IEEE Transactions on Vehicular Technology*, Vol. 64, No. 9, pp. 4215-4229, Sep. 2015.

[8] L. Wan, X. Kong, and F. Xia, "Joint range-doppler-angle estimation for intelligent tracking of moving aerial targets," *IEEE Internet of Things Journal*, vol. 5, no. 3, pp. 1625-1636, June 2018.

[9] Y. Ilyushin, A. Padokhin, V. Smolov, "Global navigational satellite system phase altimetry of the sea level: systematic bias effect caused by sea surface waves," *In Proc. 2019 PhotonIcs & Electromagnetics Research Symposium - Spring (PIERS-Spring)*, June 2019, pp. 1618-1627.

[10] B. Hammoud, F. Antreich, J. Nossek, *et al*., "Tensor-based approach for time-delay estimation," *in Proc. WSA 2016; 20th International ITG Workshop on Smart Antennas*, Mar. 2016, pp. 1-7.

[11] N. Linty, and L. Presti, "Doppler frequency estimation in GNSS receivers based on double FFT," *IEEE Trans. Veh Technol*, vol. 65, no. 2, pp. 509-524, Feb. 2016.

[12] Y. Xu, and B. Wu, "Doppler shift estimation using broadcast ephemeris in satellite optical communication," *in Proc. 2016 25th Wireless and Optical Communication Conference*, May 2016, pp. 1-4.

[13] B. Soltanian, A. Demirtas, A. Ghadam, and M. Renfors, "Reduced-complexity FFT-based method for Doppler estimation in GNSS receivers," *EURASIP J. Adv. Signal Process*, vol. 2014, no. 1, pp. 1-15, June, 2014.

[14] X. Li, X. Zhang, X. Ren, *et al*., "Precise positioning with current multi-constellation global navigation satellite systems: GPS, GLONASS, Galileo and BeiDou," *in Proc. Scientific Reports*, Sep. 2015, pp. 1-14.

[15] M. Liu, K. Li, H. Song, Y. Chen, X. Gao and F. Gong, "Using heterogeneous satellites for passive detection of moving aerial target," *Remote Sensing*, vol. 12, no. 7, pp. 1150, Apr. 2020.

[16] M. Masjedi, M. Moddares-Hashemi, and S. Sadri. "Theoretical approach for target detection and interference cancellation in passive radar," *IET Radar, Sonar Navig*, vol. 7, no. 3, pp. 205-216, Apr. 2013.

[17] X. Lu, Y. Tang, T. Wang, C. Chen, and W. Chen, "Passive radar detection based on advanced broadcasting system satellite," *in Proc. 2013 International Conference on Wireless Communications and Signal Processing*, Oct. 2013, pp. 1-4.

[18] F. Colone, R. Cardinali, and P. Lombardo, "Cancellation of clutter and multipath in passive radar using a sequential approach," *in Proc. IEEE Conf. Radar*, Apr. 2006, pp. 393-399.

[19] L. Yu, T. Qiu, and S. Luan, "Robust joint estimation for time delay and Doppler frequency shift based on generalised sigmoid cyclic cross-ambiguity function," *IET Radar Sonar Navig.*, vol. 11, no. 5, pp. 721-728, May. 2017.

[20] Z. Li, F. Santi, D. Pastina, *et al*., "Passive radar array with low-power satellite illuminators based on fractional fourier transform," *IEEE Sens. J.*, vol. 17, no. 24, pp. 8378-8394, May. 2017.

[21] X. Chen, Z. Liu, and X. Wei, "Fast FRFT-based algorithm for 3-D LFM source localization with uniform circular array," *IEEE Access.*, vol. 6, pp. 2130-2135, Dec. 2017.

[22] J. Tian, X. G. Xia, W. Cui, *et al*., "A coherent integration method via Radon-NUFrFT for Random PRI radar," *IEEE Trans. Aerosp. Electron. Syst.*, vol. 53, no. 4, pp. 2101-2109, Aug. 2017.

[23] Y. Xiao, H. Zhang, Q. Ran, *et al*., "Image encryption and two dimensional discrete M-parameter fractional Fourier transform," *in Proc. International Congress on Image and Signal Processing*, Oct. 2009, pp.1-14.

[24] S. Gao, Y. Zhong, and W. Li, "Random weighting method for multi-sensor data fusion," *IEEE Sensors J.*, vol. 11, no. 9, pp. 1955-1961, Jan. 2011.

[25] P. Xiong, M. Medley, and S. Batalama, "Spatial and temporal processing for global navigation satellite systems: The GPS receiver paradigm," *IEEE Trans. Aerosp. Electron. Syst.*, vol. 39, no. 4, pp.1471-1484, Oct. 2003.

[26] M. Raza, A. Hussain, "Maximum likelihood SNR estimation of hyper cubic signals over Gaussian channel," *IEEE Commun. Lett.*, vol. 20, no. 1, pp. 45-48, Jan. 2016.

[27] M. Liu, Z. Gao, Y. Chen, H. Song, Y. Li and F. Gong, "Passive detection of moving aerial target based on multiple collaborative GPS satellites," *Remote Sensing*, vol. 12, no. 2, pp. 263, Jan. 2020.